

Dear Author,

Please, note that changes made to the HTML content will be added to the article before publication, but are not reflected in this PDF.

Note also that this file should not be used for submitting corrections.

AUTHOR QUERY FORM

	<p>Journal: APM</p> <p>Article Number: 10238</p>	<p>Please e-mail or fax your responses and any corrections to:</p> <p>E-mail: corrections.esch@elsevier.sps.co.in</p> <p>Fax: +31 2048 52799</p>
---	--	--

Dear Author,

Please check your proof carefully and mark all corrections at the appropriate place in the proof (e.g., by using on-screen annotation in the PDF file) or compile them in a separate list. Note: if you opt to annotate the file with software other than Adobe Reader then please also highlight the appropriate place in the PDF file. To ensure fast publication of your paper please return your corrections within 48 hours.

For correction or revision of any artwork, please consult <http://www.elsevier.com/artworkinstructions>.

Any queries or remarks that have arisen during the processing of your manuscript are listed below and highlighted by flags in the proof. Click on the 'Q' link to go to the location in the proof.

Location in article	Query / Remark: click on the Q link to go Please insert your reply or correction at the corresponding line in the proof
<u>Q1</u>	Please confirm that given name(s) and surname(s) have been identified correctly.
<u>Q2</u>	Please check whether the designated corresponding author is correct, and amend if necessary.
<u>Q3</u>	The citation “Zhukovskii” has been changed to “Zhukovsky” match the author name in the reference list. Please check here and in subsequent occurrences, and correct if necessary.
<u>Q4</u>	Please check the edit made in Eq. (18), and correct if necessary.
<u>Q5</u>	This section comprises reference that occur in the reference list but not in the body of the text. Please position the reference in the text or, alternatively, delete it. Any reference not dealt with will be retained in this section.
<u>Q6</u>	One or more sponsor names may have been edited to a standard format that enables better searching and identification of your article. Please check and correct if necessary.
<u>Q7</u>	<p>The country names of the Grant Sponsors are provided below. Please check and correct if necessary. ‘RFBR’ - ‘Russia’.</p> <div data-bbox="400 1805 962 1904" style="border: 1px solid black; padding: 5px; margin-top: 20px;"> <p style="color: red;">Please check this box if you have no corrections to make to the PDF file</p> <input data-bbox="851 1819 924 1878" type="checkbox"/> </div>

Thank you for your assistance.



ELSEVIER

Contents lists available at ScienceDirect

Applied Mathematical Modelling

journal homepage: www.elsevier.com/locate/apm

Groundwater flow in hillslopes: Analytical solutions by the theory of holomorphic functions and hydraulic theory

qt Anvar Kacimov^{a,*}, Yurii Obnosov^b, Osman Abdalla^c, Oscar Castro-Orgaz^d

^a Department of Soils, Water and Agricultural Engineering, Sultan Qaboos University, Oman

^b Institute of Mathematics and Mechanics, Kazan Federal University, Russia

^c Water Research Centre, Department of Earth Sciences, Sultan Qaboos University, Oman

^d Instituto de Agricultura Sostenible, Consejo Superior de Investigaciones Científicas, Finca Alameda del Obispo, E-14080 Cordoba, Spain

ARTICLE INFO

Article history:

Received 26 May 2012

Received in revised form 9 May 2014

Accepted 3 November 2014

Available online xxx

Keywords:

Potential theory

Hodograph

Hydraulic approximation

Unconfined seepage over corner

Three-component heterogeneity

Hydrogeology of alluvium aquifers in Oman

ABSTRACT

Three 2-D steady Darcian flows in an aquifer with a subjacent confining layer of a non-constant slope or a bedding inconformity are studied by two models: a potential theory (conformal mappings, the inverse boundary-value problem method, and the theory of R-linear conjugation) and hydraulic approximation. First, flow over a corner, whose vertex is either a stagnation point or point of infinite Darcian velocity, is analysed as a transition from one “normal” regime upstream to another downstream. The hodograph domain is a circular triangle, which is mapped onto a complex potential strip via an auxiliary half-plane. Parametric equations (backwater curves) for the phreatic surface are obtained. For the same flow problem, a depth-averaged 1-D nonlinear ODE for the thickness of the saturated zone (a generalized Dupuit–Fawer model) is numerically solved showing a perfect match with the potential (2-D) solution. Second, a non-planar aquifuge boundary is reconstructed as a streamline, along which an additional “control” boundary condition holds in the form of pore pressure as a function of an auxiliary variable (a relation between the hydraulic head and vertical Cartesian coordinate). The free surface is found in terms of Cauchy’s integrals for the Zhukovskii function, with explicit integrations for selected “controls”. Third, a confined flow in a two-layered aquifer having a lens-type semi-circular inclusion in the subjacent stratum and incident velocity parallel to the interface between two aquifers is examined. The conjugation conditions along all four boundaries, across which the hydraulic conductivity jumps, are exactly met. The three velocity fields are explicitly presented, with examination of the flow net, including separatrices (“capture zone” boundaries), demarcating suction/barriering of the lens, and evaluation of the lens-induced cross-flow (commingling) between the two strata.

© 2014 Published by Elsevier Inc.

1. Introduction and hydrogeological motivation

There is a constant yearning for all that is unconfined.

F. Holderlin Mnemosyne.

* Corresponding author at: Dean’s Office, College of Agricultural and Marine Sciences, Sultan Qaboos University, P.O. Box 34, Al-Khod 123, Oman. Fax: +968 24413 418.

E-mail addresses: anvar@squ.edu.om, akacimov@gmail.com (A. Kacimov), yurii.obnosov@gmail.com (Y. Obnosov), osman@squ.edu.om (O. Abdalla), oscarcastro@ias.csic.es (O. Castro-Orgaz).

Unconfined aquifers in groundwater hydrology represent an interesting object for modeling because of a free (phreatic) surface and nonlinear boundary conditions there (see e.g., [1,2]). Mathematically, the corresponding free boundary problems are similar to ones in open channel flows [3,4]. Groundwater motion is analyzed in catchment-scale reconnaissance models or in regular annual assessment of aquifers' resources by either a hydraulic (ODE) or hydrodynamic (PDE) theoretical description ([5,6], hereafter abbreviated as PK62). The former is called the **Dupuit-Forcheheimer** (DF) model (see its recent generalizations in the so-called **Dupuit-Fawer** approximation, [7]), which in steady regimes and homogeneous rock requires solving a BVP for a second-order ODE. The latter, the potential theory -PT, calls for solving a BVP for Laplace's equation.

In arid climates with little recharge from the vadose zone to the phreatic surface, the main factor controlling its shape and locus in a relatively homogeneous aquifer is the subjacent bedrock whose geometry is commonly inferred from geological data. In the study area (Northern Oman), for which our mathematical models are developed, the geology is complex. It ranges from the Precambrian basement rocks, mainly phyllites and slates, at the bottom of the succession occupying the core of North Oman Mountains (NOM) to karstified carbonate rocks (Hajar Supergroup HSG) at the elevated areas to fractured ophiolitic sequence overlain by porous medium of Tertiary limestones and Quaternary alluvium gravel at the top of the geologic section.

The vertical cross section in Fig. 0 illustrates the field relations between the different geological units from the elevated area of NOM to the Gulf coast. The boundary between the carbonates and the ophiolites is controlled by major fault system along which several springs are originating. The Tertiary limestones and alluvium is thickening from elevated area downstream to exceed 300 m at the lower plain coastal areas and comprises the main source for groundwater production in vast areas of Northern Oman. The alluvium is deposited under alluvial and deltaic depositional environment, originates at the piedmonts of NOM and extends into the plain areas forming fan structures. The ophiolites bounding the alluvium have irregular surface ranging from steep at the NOM piedmonts to nearly planar at the coastal areas. The alluvium is predominantly composed of gravels, driven from ophiolites weathering, which vary in shape and size and mixed with fines. The portion of fines increases from the proximal to the distal part resulting in the formation of clayey silt lenses with low permeability imbedded within the alluvium. Groundwater motion there led to the precipitation of CaCO_3 and SiO_2 within the pores which enhances cementation and diagenesis processes in the lower alluvium layer leading to the formation of a cemented gravelly unit at the bottom. Therefore, the hydraulic conductivity of this unit is much less than that of the overlying unit that is predominantly composed of loose gravels. Although it is formed of similar geological material, the alluvium forms two hydrogeological units (**aquifer-aquifer** or **aquifer-aquifuge**) owing to variation in hydraulic properties due to cementation and diagenesis variation.

The recent studies of the elevation of the phreatic surface (water table) in Fig. 0 revealed its puzzling spatial variability detected in direct borehole observations and reconstructed geophysically (mostly by TDEM) (see, e.g., [8–11]). **West-East** decreasing slopes of the interfaces between different hydrogeological units (**ophiolite-carbonate-cemented gravel-gravel**) in Fig. 0 and bedrock troughs (lenses) filled with sediments of permeability contrasting with the main surrounding rock, have been found both geophysically (by seismics) and from exploratory drilling. Generally, as Fig. 0 illustrates, the water table slope is steep in the mountains and relatively mild in the valley part of the catchment (see also [12,9]). The degree of this steepness and position of the water table is vital in Oman where groundwater is the only resource for agriculture and main resource in other sectors of economy. Both traditional (falaj) and modern (tube well) water supply schemes tap unconfined aquifers by either intercepting the spring discharge or relatively shallow water table in Fig. 0.

In this paper we answer the following questions: **(a) How** to accurately describe groundwater dynamics in aquifers with non-planar bedrock as in Fig. 0? **(b) When** a relatively simple DF model is suitable and what is its error as compared with the PT?

In standard DF or PT models the bedrock boundary of an unconfined aquifer is assumed to be planar and either absolutely impermeable (aquifuge) or slightly permeable (aquitard) but with leakage properties constant throughout the whole

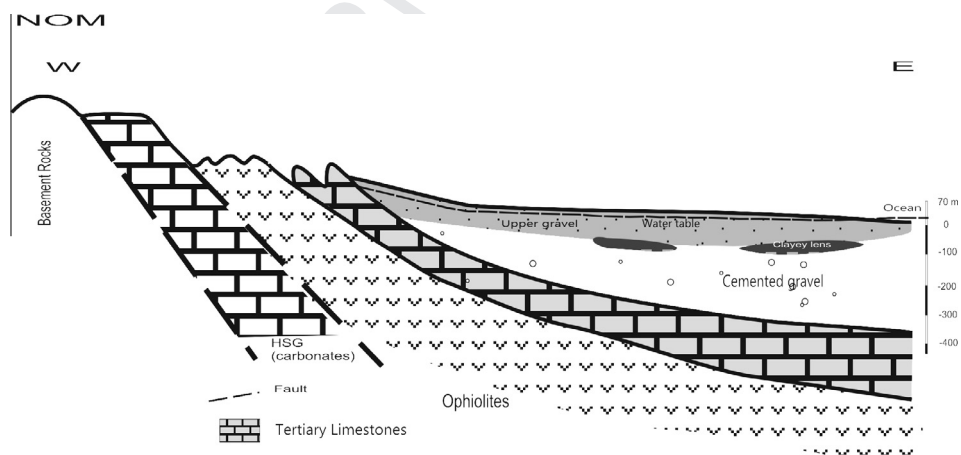


Fig. 0. Typical hydrogeological cross-section of a coastal aquifer in Northern Oman.

groundwater flow domain (PK62, [1]). Kacimov [13] attributed steep slopes of the free surface to “groundwater fall” geometry of the bedrock, i.e. a non-planar aquifuge boundary making a step-down (similar to a drop-structure in classical hydraulics, [3]). In hillslope hydrology, both the DF and PT models are used (see, e.g. [14–19]) but explicit closed-form solutions (like ours below) to phreatic-surface flow problems are rare. Dachler and Gersevanov [20,21] (abbreviated as DG below) studied analytically aquifers whose bedrock tilts at a constant angle $\alpha\pi$, $0 \leq \alpha \leq 1/2$ (Fig. 1a). DG’s results obtained by PT at small α matched well the DF approximation. DG involved two analytical approaches in solving BVPs: the hodograph method and functional equations (see PK62), which in their own turn are based on the theory of holomorphic functions.

In this paper we extend the model of Kacimov [13] and consider the following bedrock “anomalies”: (a) an aquifer with an underlying aquifuge whose inclination changes abruptly from aquifer’s upstream to downstream (Fig. 1a); (b) an aquifuge with a continuously varying slope (Figs. 1c and 4a); (c) a system of two commingled aquifers which have a permeable lens through which an intricate “diversion” flow from one aquifer to another occurs (Fig. 6). Correspondingly, we apply four different

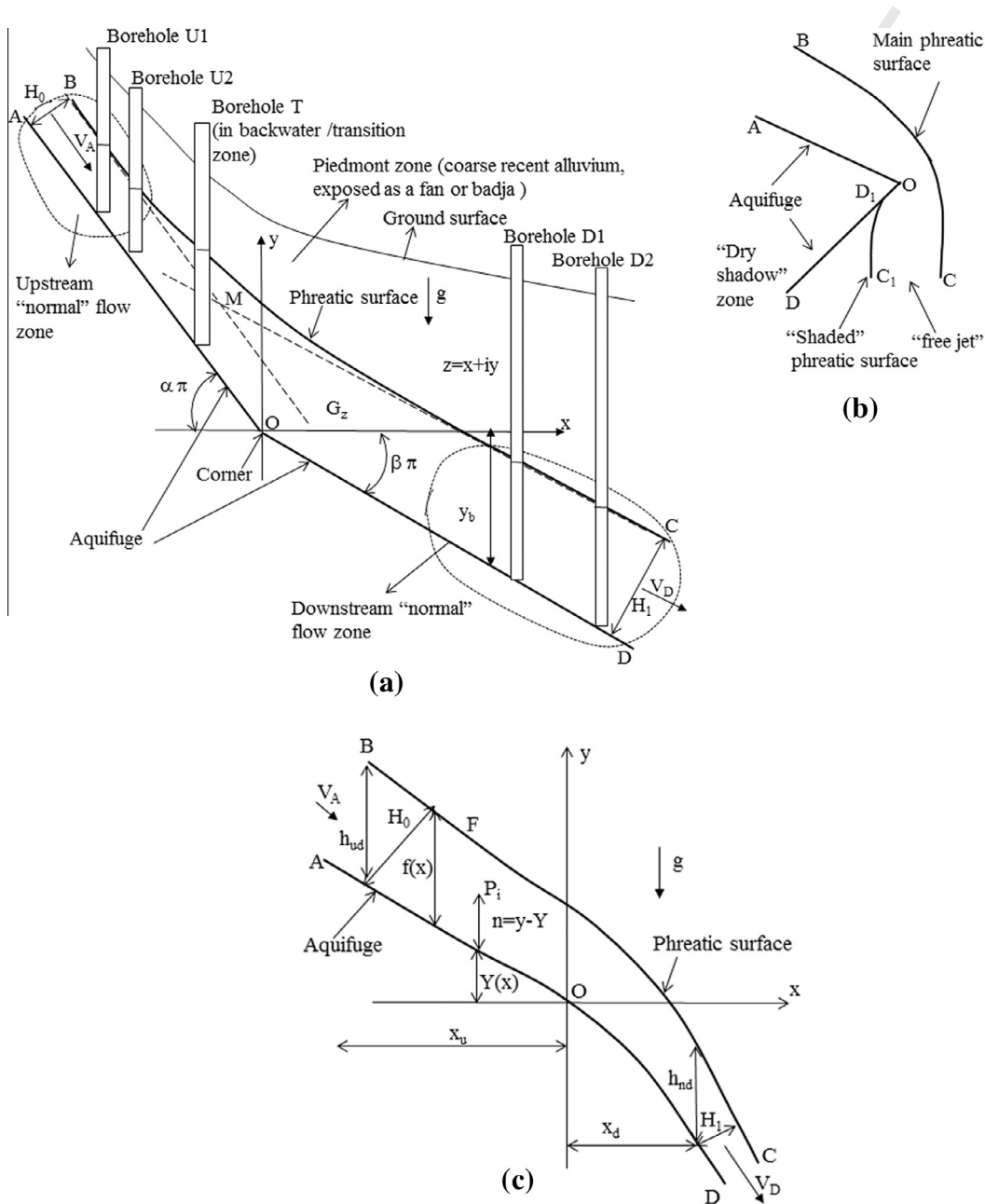


Fig. 1. Flow over a common corner-shaped aquifuge, physical domain (a); geologically exotic case with a “free groundwater jet” beneath a corner (b); flow over a curved bedrock (c).

techniques: the hodograph method [13,22,23], hydraulic approximation [24], boundary-value problem method [25,26] and the theory of boundary-value problems of R-linear conjugation [27] – all of them springing from the arsenal of PK62.

We assume a Darcian flow, ignore the capillary fringe, accretion or evapotranspiration to/from the vadose zone and any sinks-sources (e.g. pumping wells) in the flow domain. Within a given hydrostratigraphic unit (aquifers, lens in Fig. 0) the hydraulic conductivity is constant.

2. 2-D flow over a bedrock wedge

In this section we assume that the hydraulic conductivity of the upper gravel, k , is much higher than that of the cemented gravel such that the interface, AOD , between the two in Fig. 0 is a no-flow boundary. This assumption is acceptable for common conductivity ratios of 10–50 of the two hydrostratigraphic units. We assume that AOD makes a corner (Fig. 1a). The origin of a Cartesian coordinate system coincides with the vertex O . The flanks of the wedge OD and AO dip at angles $\alpha\pi$ (counted from Ox positive clockwise) and $\beta\pi$ (positive counterclockwise), correspondingly. Without any loss of generality we consider here the “hillslope” case of $0 < \alpha = \text{const} < 1/2$, $0 < \beta = \text{const} < 1/2$. If $\alpha > \beta$ flow decelerates downstream of the transition zone near point O , otherwise it accelerates. The flow rate (per unit length perpendicular to the plane of Fig. 1a) in the upper gravel of Fig. 0 is Q .

Dachler [20] (see his Fig. 48) obtained a PT solution to the flow problem in Fig. 1a for $\alpha = -1/2$, $\beta = 1/2$; Kacimov and Li et al. [13,28] studied the case of $\alpha = 0$, $\beta = 1/2$. Strack [1] (see his Figs. 5.22, 6.31, 6.32, 6.43, 7.15, 7.28, 7.29, 7.30) considered winding seepage in domains with sharp-edged impermeabilities. To the best of our knowledge, no attempts have been made to address the general case of arbitrary α and β in Fig. 1a.

If $\alpha > 0$ and $\beta < 1/2$ (Fig. 1a), then the phreatic surface BC far upstream and downstream of O is parallel to the bedrock. We will call this 1-D unidirectional flow “normal” (analogously to corresponding open channel flows, [3]). The “normal” saturated zone thicknesses are H_0 and H_1 far above and below point O , respectively. The corresponding zones are schematically demarcated by dotted lines in Fig. 1a. In these zones flow is aligned with the bedrock, the 1-D DF approximation works well and gives exactly the same solution as PT. In the conjugation zone of Fig. 1a, the free surface BC is essentially non-straight and 2-D analysis by PT is needed.

At $\alpha = \beta$ flow is trivially unidirectional, with BC everywhere parallel to AOD [20]. Dashed lines in Fig. 1a represent the “primitive” phreatic surface corresponding to two “normal” flows at constant slopes $\alpha\pi$ and $\beta\pi$, i.e. the straight lines $y = -\tan \alpha\pi x + H_0/\cos \alpha\pi$ and $y = -\tan \beta\pi x + H_1/\cos \beta\pi$. The “primitive” lines intersect at the point M and the corresponding “phreatic corner” BMC would be a simplistic Dupuit replica of AOD , translated. Our objective is to find how the angularity of AOD affects the shape of BMC if PT is used.

In a common manner (PK62) we introduce a complex physical coordinate $z = x + iy$, hydraulic head $h(x, y)$, Darcian velocity vector $\vec{V} = -k\nabla h$, velocity potential $\phi = -kh$, stream function ψ , complex potential $w = \phi + i\psi$ and complexified Darcian velocity $V = u + iv$. ϕ , ψ and h are harmonic and $\phi + ky = 0$ along BC . We are free to select O as a fiducial point i.e. to choose $\phi_O = 0$ and $\psi_{AOD} = 0$ (and, hence, $\psi_{BC} = Q$).

In the w -plane the strip G_w (Fig. 2a) corresponds to the flow domain G_z in the z -plane. In the hodograph plane, G_z is imaged by a circular triangle G_v depicted in Fig. 2b. Here the case of $\alpha > \beta$ is illustrated with O being a stagnation point. Obviously, if $\alpha < \beta$ then $V_O = \infty$ i.e. the hodograph trigon is infinite.

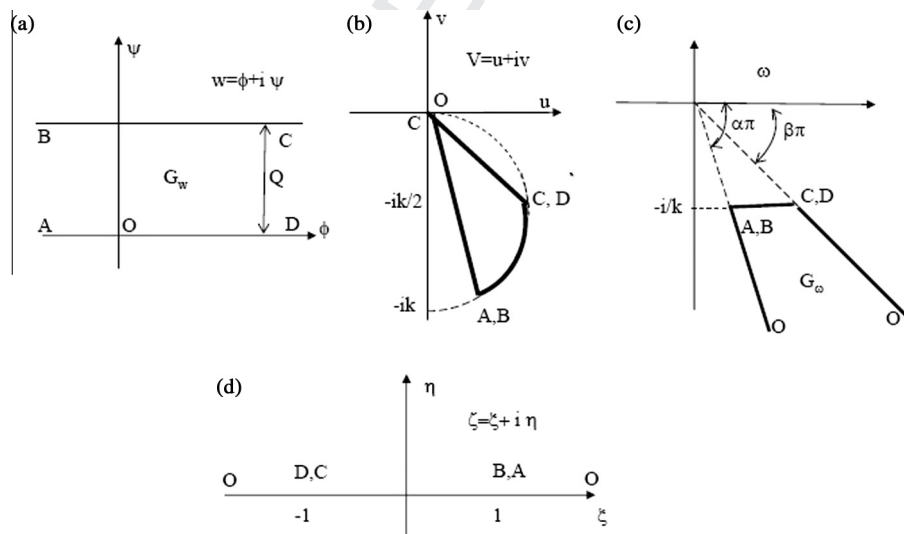


Fig. 2. Complex potential domain (a), hodograph domain (b), inverted hodograph domain (c), auxiliary plane (d) corresponding to the flow domain in Fig. 1a.

Obviously, the magnitudes of velocities in the “normal” flow zones of Fig. 1a are $|V_A| = |V_B| = k \sin \alpha\pi$ and $|V_C| = |V_D| = k \sin \beta\pi$. Clearly, $Q = H_0|V_A| = H_1|V_D|$.

As is well known, $V(z)$ is an antiholomorphic function and $u - iv = dw/dz$ is holomorphic. We use the method of inversion (PK62) and invert G_w into a trigon G_ω where $\omega = dz/dw$ (Fig. 2c). Obviously, if $\alpha < \beta$ then G_ω in Fig. 2c is a standard triangle.

Now we map conformally G_w onto G_ω via an auxiliary plane $\zeta = \xi + i\eta$ (Fig. 2d) using the Schwarz–Christoffel formula twice. Namely, first we map G_w onto the half-plane $\text{Im}\zeta > 0$ of Fig. 2d by the function

$$w(\zeta) = \frac{Q}{\pi} \ln \frac{\zeta - 1}{\zeta + 1}, \tag{1}$$

where the logarithm’s branch is fixed by the condition of its negativeness at $\zeta = \xi > 1$ and therefore the correspondence of points is $D, C \rightarrow -1, A, B \rightarrow 1, O \rightarrow \infty$.

The second mapping is

$$\omega(\zeta) = a_1 \int_{-1}^{\zeta} (1 + \tau)^{-\beta} (1 - \tau)^{\alpha-1} d\tau + \omega_D, \tag{2}$$

where τ is a dummy variable, and a_1 and ω_D are the two Schwarz–Christoffel constants. Obviously, from Fig. 2c $\omega_D = (\cot \beta\pi - i)/k$ and $\omega_A = (\cot \alpha\pi - i)/k$. Then from (2) at $\zeta = 1$ we express

$$a_1 = \frac{\cot \alpha\pi - \cot \beta\pi}{kI_1}, \quad I_1 = \int_{-1}^1 (1 + \tau)^{-\beta} (1 - \tau)^{\alpha-1} d\tau. \tag{3}$$

The integral in (3) is expressed as:

$$I_1 = 2^{1-\beta} B(1 - \beta, \alpha),$$

where $B(x, y)$ is the Beta-function. Combining Eqs. (1) and (2) we get

$$z(\zeta) = \int_{-\infty}^{\zeta} \frac{dz}{dw} \frac{dw}{d\zeta} d\zeta = \frac{Q}{2\pi} \int_{-\infty}^{\zeta} \frac{\omega(\zeta)}{\zeta^2 - 1} d\zeta. \tag{4}$$

Both the rays AO, OD , and phreatic surface BC in the z -plane are obtained as images of the intervals $(1, \infty), (-\infty, -1)$ and $(-1, 1)$, correspondingly, in the ζ -plane. Now we simplify the computations by transforming the mapping function (4).

First, we note that the function (2), which is the numerator of the integrand in (4), has the following representations near the points $\zeta = \pm 1$:

$$\omega(\zeta) = \omega_D + (\zeta + 1)^{1-\beta} \omega_{-1}(\zeta), \quad \omega(\zeta) = \omega_A + (\zeta - 1)^\alpha \omega_1(\zeta),$$

where the functions $\omega_{\pm 1}(\zeta)$ are holomorphic and not vanishing in the corresponding vicinities of the points $\zeta = \pm 1$. Consequently, the integral (4) at its singular points $\zeta = \mp 1$ has the jumps $i\pi\omega_D/2$ and $-i\pi\omega_A/2$. Therefore, the mapping functions for OD, BC , and AO can be successively found as follows:

$$z(\xi) = \frac{a_1}{2} \left(\ln \frac{\xi + 1}{\xi - 1} \int_{\xi}^{-1} (-t - 1)^{-\beta} (1 - t)^{\alpha-1} dt - \int_0^{-1/\xi} (1 - t)^{-\beta} (1 + t)^{\alpha-1} t^{\beta-\alpha-1} \ln \frac{t+1}{t-1} dt \right) - \frac{\omega_D}{2} \ln \frac{\xi + 1}{\xi - 1}; \tag{5}$$

$$z(\xi) = \frac{a_1}{2} \left(e^{-i\pi\beta} c_1 + \ln \frac{1 - \xi}{1 + \xi} \int_{-1}^{\xi} (1 + t)^{-\beta} (1 - t)^{\alpha-1} dt - \int_{-1}^{\xi} (1 + t)^{-\beta} (1 - t)^{\alpha-1} \ln \frac{1 - t}{1 + t} dt \right) - \frac{\omega_D}{2} \left(\ln \frac{1 - \xi}{1 + \xi} + i\pi \right), \tag{6}$$

where

$$c_1 = \int_0^1 (1 - t)^{-\beta} (1 + t)^{\alpha-1} t^{\beta-\alpha-1} \ln \frac{1 - t}{1 + t} dt;$$

$$z(\xi) = \frac{a_1}{2} \left(e^{-i\pi\beta} c_1 - c_2 + \ln \frac{\xi - 1}{\xi + 1} \left(I_1 - \int_1^{\xi} (1 + t)^{-\beta} (1 - t)^{\alpha-1} dt \right) + e^{-i\pi\alpha} \int_1^{\xi} (1 + t)^{-\beta} (t - 1)^{\alpha-1} \ln \frac{t - 1}{t + 1} dt \right) + \frac{\omega_D}{2} \times \ln \frac{\xi - 1}{\xi + 1} + i\pi \frac{\omega_D - \omega_A}{2}. \tag{7}$$

We recall that I_1 is defined in (3) and

$$c_2 = \int_{-1}^1 (1 + t)^{-\beta} (1 - t)^{\alpha-1} \ln \frac{1 - t}{1 + t} dt.$$

The last equations are obtained by changing the order of integration in (4) and by making the substitution $\pm 1/t \rightarrow t$ in the integrals with infinite limits $\pm\infty$.

Note, that the first integrals into all three formulae (5)–(7) can be expressed in terms of an incomplete Beta-function $B_x(a, b)$, or a hypergeometric function $F(a, b; c; z)$, i.e.

$$\int_{\xi}^{-1} (-t-1)^{-\beta} (1-t)^{\alpha-1} dt = \frac{2^{\alpha-1} (-\xi-1)^{1-\beta}}{\beta-1} F(1-\alpha, 1-\beta; 2-\beta; (1+\xi)/2).$$

Analogous representations could be obtained for the first integrals in (6), (7).

The parametric equations of BC are obtained by separation of the real and imaginary parts in the expressions for $z(\zeta)$ given by (6). The rays making the aquifuge are plotted by (5) and (7). In computations we used the **NIntegrate** routine of *Mathematica* [29] for evaluation of the corresponding integrals. These integrals are improper but are computed well with a standard assessment of errors.

We introduce dimensionless quantities $(x^*, y^*) = 2\pi k/Q (x, y)$ and drop the superscript *. Fig. 3a presents the phreatic surface plotted at $\beta = 0.1$ and $\alpha = 0.35$ and – for comparisons – the “primitive” BMD (plotted as a dashed wedge). Fig. 3b shows phreatic surfaces calculated for $\alpha = 0.3$ and $\beta = 0.25, 0.2$ and **0.15** (curves 1–3, correspondingly), i.e. a steep slope jumping to a mild one downstream. In Fig. 3c the phreatic surfaces are plotted for $\beta = 0.15$ and $\alpha = 0.2, 0.25$ and **0.35** (curves 1–3, correspondingly).

In our model, the behavior of velocity at infinity upstream (points A–B, Fig. 1a) and downstream (points C–D) was “normal”. Velocity at one or both of these two extremes can vanish, that corresponds to infinite saturated depths of the aquifer and infinite pore pressure at these two points. Mathematically, one or two free parameters emerge in the solution. This reflects the unbounded geometrical extension of the flow domain and, consequently, lack of knowledge (mathematical ignorance) of the details of the recharge–discharge zones (located far upstream–downstream of point O in our Fig. 1a). For example, Dachler’s (1936, see his pp. 98–100, Abb. 48) upstream velocity at infinity is zero and his solution is one-parametric. PK-62 elaborated several ways of fixing this/these parameters. The technique of solving the BVP (the hodograph method), does not depend on these free parameters and the modes of fixation. The free parameters emerge in both PT and DF models.

Similarly to open channel hydraulics [3], we call BC a backwater curve. Let a network of monitoring wells be drilled as schematically depicted in Fig. 1a. These wells serve for piezometric mapping. In wells (U1,U2) (and any other wells in the “normal” upstream zone), the depth of water counted from the aquifuge ($H_0/\cos\alpha\pi$) and phreatic surface slope “mimic” the dip of the aquifuge. Similarly, piezometric data from wells (D1,D2) (Fig. 1a) in the downstream “normal” zone are a replica of the geological bedding there. A well (T in Fig. 1a) drilled in the backwater zone is, however, different. As our computations in Fig. 3 illustrate, the water level there overshoots the “normal” level inferred (and extrapolated) from wells (U1, U2). Well T (if drilled to the aquifuge) detects the same α as U1 and U2 and the constancy of α in all three wells (U1, U2, T) can be alternatively corroborated by, say, seismics geophysics. However, the corner (downstream of well T) acts as a “hydraulic leaven” i.e. in well T the free surface of groundwater flow is significantly higher compared with the normal which one would draw based on the DF model and readings from the upstream wells (U1,U2). Actually, the overshoot of the phreatic surface is a precursor to the change of bedrock dip downstream of well T.

Thus, attributing the piezometric data to the simplistic geometry of the bedrock should be caveated. “Abnormalities” of the phreatic surface, which are routinely mapped by standard interpolations of water level readings in the wells can be also caused by other than the non-planar geometry of the bedrock, e.g. by faults, transition from an aquifuge to an aquitard with leakage, or localised lenses (Fig. 0) as in Section 4 below.

Inverse problems of reconstructing the bedrock from the locus of the phreatic surface call for subtle skills to tinker with the dearth of data (often recondite or spurious) gleaned from geology, hydrogeology and geophysics. In contrast, in open-channel hydraulics “abnormalities” of the free surface are directly measured and can be attributed to the sudden changes of the channel bed geometry, roughness, or channel cross-sectional area [3].

3. 1-D model of flow over a curved bedrock

In this section we utilize a hydraulic approximation for a phreatic surface flow over an arbitrary curved bedrock $Y(x)$. We do not consider geologically exotic cases like one in Fig. 1b where a dry shadow zone emerges with a free jet of groundwater demarcated by two phreatic surfaces but rather study a common situation shown in Fig. 1c, with $Y(x)$ being a sufficiently smooth function. The aim is to find the elevation, $f(x)$, of the phreatic surface over the bedrock. For a while, we return to dimensional coordinates.

Castro-Orgaz et al. [24] obtained higher order 1-D groundwater flow hydraulic theory using depth-averaging and systematic application of Picard’s iteration. For the flow in Fig. 1c the theory yields (see Appendix A):

$$\frac{Q}{kf} \left(1 + f_x Y_x + Y_x^2 + \frac{ff_{xx} + f_x^2}{3} \right) + f_x + Y_x = 0 \quad (8)$$

with respect to $f(x)$. In Eq. (8) the subindex x indicates differentiation. The required smoothness of $Y(x)$ is clear from Eq. (8). Appendix A outlines the proof of Eq. (8).

Eq. (8) was integrated for the case of a wedge from the previous section. The second Picard iteration cycle needs a bed function $Y(x)$ continuous at least up to its second derivatives. In the wedge problem this condition is violated at point O in Fig. 1. This limitation was obviated in the numerical solution by forcing continuity of the free surface slope at this point ($x = 0$), that is, by assuming $\tan\alpha + n_{x-} = \tan\beta + n_{x+}$ there.

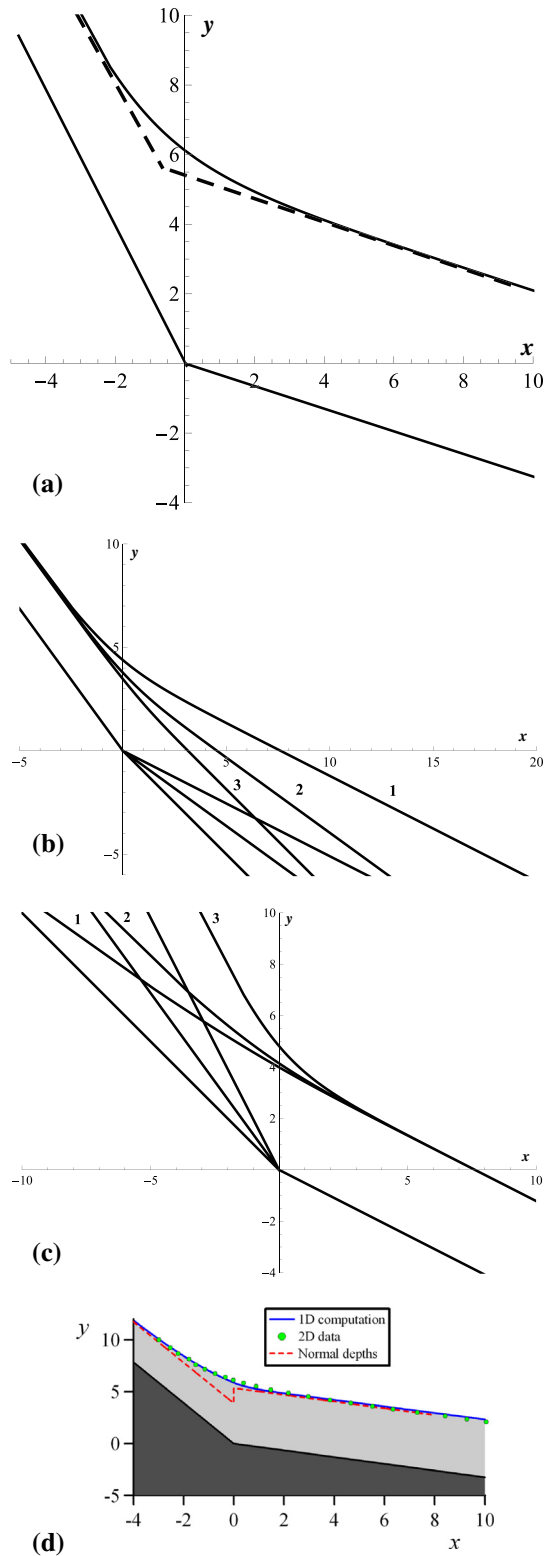


Fig. 3. Phreatic flow boundaries at $\beta = 0.1$ and $\alpha = 0.35$, and “primitive” BMD (plotted as a dashed wedge) (a); phreatic surfaces for $\alpha = 0.3$ and $\beta = 0.25, 0.2$ and 0.15 (curves 1–3, correspondingly) (b); phreatic surfaces for $\beta = 0.15$ and $\alpha = 0.2, 0.25$ and 0.35 (curves 1–3, correspondingly) (c); comparisons of the phreatic surface obtained by PT (blue curve), hydraulic theory (green dots) and “normal” depth rays (red dashed lines) for $\alpha = 0.35, \beta = 0.1$ (d). (For interpretation of the references to color in this figure legend, the reader is referred to the web version of this article.)

Upstream of the wedge at $x = x_u$, where $|x_u|$ is large enough, we set a flow depth $f_u = m_n f_{nu}$, with m_n a parameter close to unity. This is to account that the value of f_n at $x = x_u$ is slightly different from $H_0 / \cos \alpha \pi$ (see Fig. 1a), which is the asymptotic analytic value at infinity. At x_u we have $f_x \approx 0$. With these two left-side boundary conditions Eq. (8) was numerically tackled by a 4th-order Runge-Kutta method until reaching a section $x = x_d$ ($|x_d|$ should be large enough) on the downstream slope of the wedge. The computed value of the flow depth at this section is f_d . For a physically correct solution f_d must be close to $f_{nd} = H_1 / \cos \beta \pi$. Thus, the value f_u was iterated until reaching a value of f_d close to f_{nd} , keeping f_u close to f_{nu} .

A code was written in Vbasic. The results of numerical integration are shown in Fig. 3d for $\alpha = 0.35$, $\beta = 0.1$ in dimensionless variables of the previous section, i.e. $(x, y) = (x, y)\pi K / (2Q)$. We selected $x_u = -10$ and $x_d = +10$, respectively. The corresponding normal depths were $f_{nu} = 3.883246$ and $f_{nd} = 5.344798$. The starting values for the numerical integration at the upstream section were $f_x = 0$ and $f = m_n f_{nu}$, with m_n undetermined. Computations were initiated with $m_n = 1.001$, thereby reducing it as iteration progressed. The final iterated value was $m_n = 1.000529$, resulting at $x = +10$ the flow depth $f = 5.57044$. As one can see from Fig. 3d, the 1-D hydraulic model is in excellent agreement with the 2-D potential solution.

4. PT model for flow over a curved bedrock

In this section we again use PT but consider an impermeable boundary AOD as an arbitrary curve shown in a vertical cross-section of Fig. 4a. Although the geological section in Fig. 0 depicts the bedrock as a smooth monotonic positively-concave curve, below this is mathematically not necessary.

Curved beds of open channels have been theoretically tackled both in the hydraulic approximation (the Poincare-Masse-Jaeger analysis, see, e.g., [3]) and in terms of PT (see e.g. [30,31]). A transition from one constant-slope “normal flow” to another was assumed to be along a straight line, polygon, circular arc or another specified curve modeling the channel bed contour (see, e.g., [32,3]). Pressure exerted by flowing water onto the channel bed is then calculated from the solution [31]. The varying water depths and velocities are experimentally measured.

In the previous section we have already used the hydraulic model of Castro-Orgaz et al. [24] for a given bedrock boundary $Y(x)$. In this section we not only recur to a full 2-D model but also use an inverse approach. Namely, instead of specifying the curve AOD in Fig. 4a, we specify a pressure distribution there. Then we reconstruct both the phreatic surface BFC, which is (like in the two previous sections) a streamline and isobar, and the bedrock geometry itself. Such an “inverse” BVP is

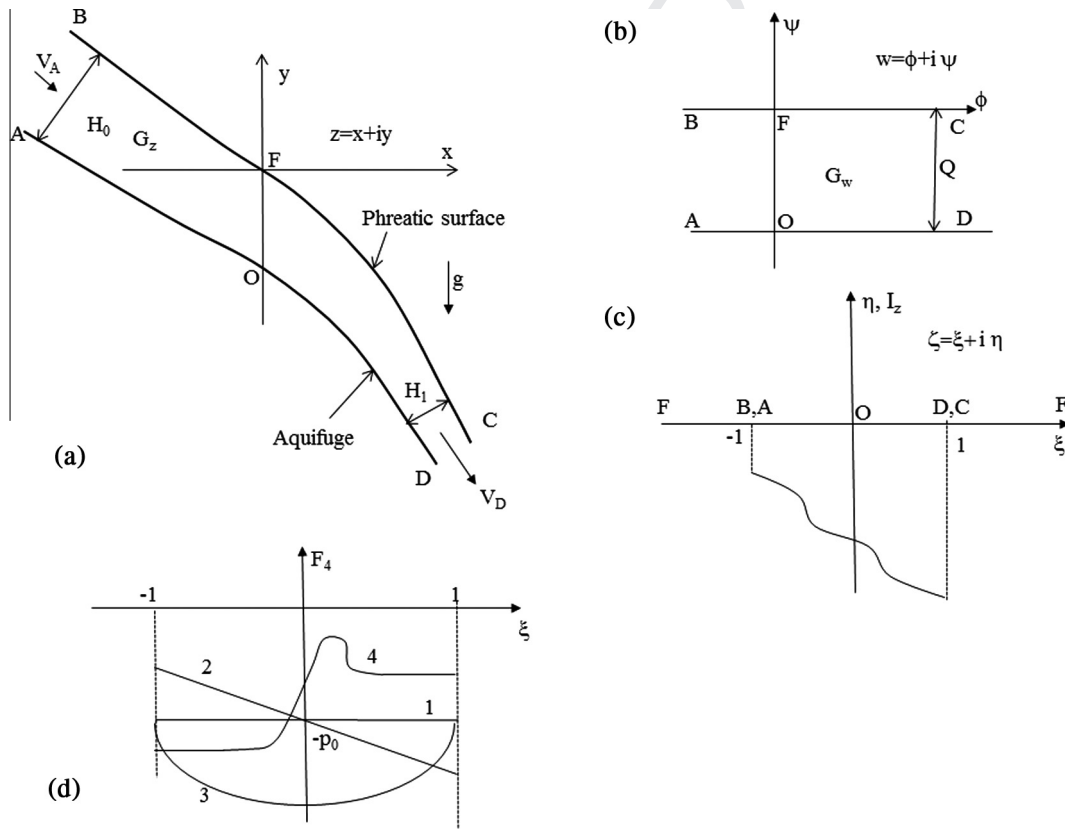


Fig. 4. Phreatic flow over a curved aquifuge, physical domain (a); complex potential domain (b); auxiliary plane (c); control functions in the auxiliary plane: “normal” 1-D flow (line 1), linear pressure variation (line 2), semi-elliptical variation (curve 3), two “normal” flows conjugated through a “kink”(d).

“constructal” and has been used for designing flow domains with desired or optimal integral and local field characteristics [33,10,34,26].

The G_w domain is shown in Fig. 4b. Point F there is fiducial ($w_F = 0$) and we select Cartesian coordinates x_Fy . Along the aquifuge contour $\psi = -Q$. We repeat: none of the boundaries of G_z is known in advance.

We map G_w conformally on the half-plane $\zeta > 0$ in Fig. 4c by the function:

$$w(\zeta) = -\frac{Q}{\pi} \ln \frac{\zeta - 1}{\zeta + 1}. \tag{9}$$

Several options for a characteristic “control” function along AOD are available (see, e.g., [33]). Here we specify one of the following distributions along AOD:

$$h = F_1(y), \quad \text{or } p = F_2(y), \quad \text{or } y = F_3(h), \tag{10}$$

where p is the pore pressure head defined as $p = -(\phi/k + y)$ (see PK62) and F_1, F_2 , or F_3 are the control functions whose smoothness will be elaborated later.

We introduce a holomorphic Zhukovsky function $Zh = z + iw/k = (x - \psi/k) + i(\phi/k + y)$, $R_z = \text{Re}[Zh]$, $I_z = \text{Im}[Zh]$, i.e. the imaginary part of Zh is $-p$. The boundary conditions for Zh in the G_z plane of Fig. 4a and auxiliary plane of Fig. 4c are

$$I_z = 0 \text{ along BF, } -\infty < \xi < -1, \quad \text{and along FC, } \infty > \xi > 1, \tag{11}$$

$$I_z = F_4(\xi) \text{ along AD, } -1 < \xi < 1,$$

where $F_4(\xi)$ is a given function (see Fig. 4d) related to one of the three forms in Eq. (10).

Along AOD from Eq. (1)a

$$\phi = -Q/\pi \log[(1 - \xi)/(1 + \xi)], \quad -1 < \xi < 1.$$

At $\zeta = \infty$ the Zhukovsky function nullifies because we have selected point F as a fiducial for w (Fig. 4b) and as the origin of physical coordinates (Fig. 4a). Consequently, we have to find $Zh(\zeta)$ based on the Dirikhlet conditions (11). An integral solution to this BVP is (see, e.g., PK62):

$$Zh(\zeta) = \frac{1}{\pi} \int_{-1}^1 \frac{F_4(\tau)}{\tau - \zeta} d\tau + R_{zF}, \tag{12}$$

where the constant $R_{zF} = 0$ owing to the fiduciality of point F . Now a smoothness requirement on F_4 can be identified: for the singular integrals in Eq. (12) to exist it is sufficient for F_4 to belong to the Holder class (PK62). Integral representation (12) and its generalizations for mixed and Riemann–Hilbert problems have been widely used in modeling direct and “inverse” problems for Darcian and ideal fluid flows (see e.g. [10], PK62, [35]).

We apply the Sokhotskii formulae (PK62) to (12) and (9). Then the parametric equations of AOD are:

$$x = \frac{1}{\pi} V.P. \left[\int_{-1}^1 \frac{F_4(\tau)}{\tau - \xi} d\tau \right] - \frac{Q}{k}, \quad y = F_4(\xi) + \frac{Q}{k\pi} \log \frac{1 - \xi}{1 + \xi}, \quad |\xi| < 1. \tag{13}$$

The phreatic surface is described by:

$$x = \frac{1}{\pi} \int_{-1}^1 \frac{F_4(\tau)}{\tau - \xi} d\tau, \quad y = \frac{Q}{k\pi} \log \frac{\xi - 1}{\xi + 1}, \quad |\xi| > 1, \tag{14}$$

where V.P. stands for the principal value. In Eq. (13) the integral is of the Cauchy type, i.e. is singular, while in Eq. (14) the integral is regular. Correspondingly, the CauchyPrincipalValue or NIntegrate as Mathematica routines should be used for arbitrary F_4 in evaluation of the integrals.

Obviously, if $F_4 = -p_0 = \text{const}$ (Fig. 4d, line 1) then we arrive at Dachler’s case (see his Fig. 45) of a “normal” unidirectional flow over a planar aquifuge of a constant tilt and phreatic surface parallel to it.

Let us select $F_4(\xi) = -p_0 - e\xi$ (Fig. 4d, line 2) where p_0 is a given positive pressure head at point O , i.e. we specify a linear pressure distribution as a function of an auxiliary variable. The linearly varying $F_4(\xi)$ in the integral of (12) corresponds to $y = 2p_0 - \phi + 2e \tanh \phi/4$, i.e. is in the form of F_3 in Eq. (10).¹ In G_w at point O $\phi = 0$ and, hence, $y = -p_0$ in G_z ; e is a given constant. Obviously, the diad (p_0, e) is constrained by the inequalities $(p_A > 0, p_D > 0)$.

We introduce dimensionless quantities $(x^*, y^*, \phi^*) = 2\pi k/Q * (x, y, \phi)$, $(p_0^*, e^*) = \pi k/Q * (p_0, e)$ and drop the superscripts. The shapes of AOD and BFC are found from (14) by integration as:

$$x = -2(p_0 - \xi e) \ln \frac{1 - \xi}{1 + \xi} - 4e - 2\pi, \quad y = 2 \ln \frac{1 - \xi}{1 + \xi} - 2p_0 - 2e\xi, \quad |\xi| < 1, \tag{15}$$

¹ A similar linear relation between $\sin \theta$ (θ is the angle between the velocity vector and abscissa axis) and an auxiliary variable of a half-plane was assumed by Zhukovskii [36] such that he reconstructed his $w(z)$ in a parametric form. Similarly (but numerically) [37] reconstructed a free surface segment.

$$x = -2(p_0 + \zeta e) \ln \frac{\zeta - 1}{\zeta + 1} - 4e, \quad y = 2 \ln \frac{\zeta - 1}{\zeta + 1}, \quad |\zeta| > 1, \tag{16}$$

correspondingly.

Fig. 5a illustrates the free surfaces calculated for $(p_0, e) = (1, 0.2)$, $(2, 0.2)$ (curves 1 and 2, respectively) plotted by Eq. (15) and the corresponding aquifuge boundaries (curves 3 and 4) by Eq. (16). In Fig. 5b we plotted the flow domains for a groundwater fall with a curved bedrock. For this reconstruction we selected a linear $F_4(\xi)$ (see Fig. 3d) with $(p_0, e) = (1, -1)$, $(2, -2)$ such that pore pressure at point D nullifies, i.e. the “dangling” tail of G_z is at atmospheric pressure. As one moves down in Fig. 5b, the “confining” action of the bedrock decreases and eventually a free “jet” of groundwater “falls” vertically. In Fig. 5b phreatic surfaces for the two diads are curves 1 and 2 and the aquifuge boundaries are curves 3 and 4, (all double-correspondingly plotted by Eqs. (15), (16)). As is evident from Fig. 5b, AOD is not necessary a function in the sense of $y(x)$ (see also Fig. 1b), albeit AFC is. Curves 3 and 4 have protruding tips where the Darcian velocity reaches its maximum and, correspondingly, the thickness of the saturated zone reaches its minimum (similarly to the abrupt drop-down in [13]). Unlike free heavy jets in open-channel flows [38], groundwater close to point D (C) in Fig. 5b acquires a constant velocity k .

Fig. 5c presents the reconstruction of G_z for another control function: $F_4 = -p_0 - e_1 \sqrt{1 - \xi^2}$ (schematically shown as curve 3 in Fig. 4d). Curves 1 and 2 are the free surfaces and curves 3 and 4 are the bedrock contours calculated for two diads $(p_0, e_1) = (1, 1)$, $(0, 1)$, double-correspondingly. Again the curves 2 and 4 give the case of another groundwater fall but here – unlike Fig. 5b – both far downstream and upstream we have $p = 0$ and, therefore, “free jet” conditions.

Other “controls” $F_4(\xi)$ can be selected, e.g. as curve 4 in Fig. 4d, which has two flat segments corresponding to “normal” flows upstream and downstream and a “kink” (analogous to ones in Figs. 5, of [31]). One can also select $\phi - cy = C$ specified at a certain segment $-1 < -\xi_0 < \xi < \xi_1 < 1$ of AD . This segment will then correspond to an interface between a relatively light moving groundwater and static DNAPL beneath the interface, with c expressed through the density contrast and C through the pressure in the entrapped DNAPL (see [13,22,25,23]). Similarly to [39], a “reattached” finite-size phreatic surface [40] with a segment $p = 0$ along $-1 < -\xi_2 < \xi < \xi_3 < 1$ can be introduced into G_w through F_4 .

The choice of “controls” F_4 , even within the Holder class, should be admonished: the found shape AOD has to be checked *a posteriori*, from both a physical and geological viewpoint. Indeed, fancy shapes in G_z (AOD with “loops”, or two-list Riemann surfaces) as integral outcomes of a “desired” F_4 can emerge. This is a common price paid by both this “inverse” [33] and Gersevanov’s techniques (we recall that [21] used an alternative inverse approach to design G_z in unconfined phreatic flows). It is still not clear what kind of isoperimetric/optimal shape design problems similar to Bejan, Kacimov and Kacimov et al. [41,10,26] can be solved by “controls” of this kind.

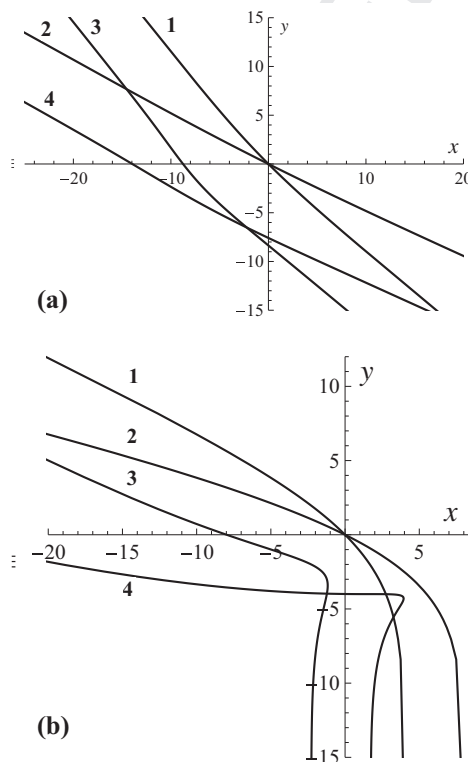


Fig. 5. Phreatic surfaces (curves 1 and 2) and aquifuge boundaries (curves 3 and 4) calculated for: linear control functions $F_4(\xi)$ with $(p_0, e) = (1, 0.2)$ and $(2, 0.2)$ (a); linear control functions $F_4(\xi)$ with $(p_0, e) = (1, -1)$ and $(2, -2)$ (b); semi-elliptical control functions $F_4(\xi)$ with $(p_0, e_1) = (1, 1)$ and $(0, 1)$ (d).

378 Is there an advantage of our integral solution as compared with one of Gersevanov, who solved a finite difference equation
 379 in terms of $z = f(w)$? We believe, yes, because F_4 allows for an *a priori* assessment of the pore pressure in the whole flow
 380 domain (Gersevanov's reconstruction of G_z was purely mathematical). Indeed, $p(x, y)$ is a harmonic function and therefore
 381 obeys the maximum principle (PK62). Consequently, the maximum of a selected $|F_4|$ in Fig. 4d bounds from above the pore
 382 pressure head everywhere in G_z . Still another "constructual" technique can be implemented by specifying a Darcian velocity
 383 magnitude along AOD and, consequently, fixing a hodograph domain (see e.g., [42]). A simple assessment of effective stresses
 384 and seepage forces - prior to solving the flow problem - is important in the analysis of hillslope stability.

385 **5. Flow in two aquifers commingled via a depositional trough**

386 In this section we abandon the assumption on impermeable bed of G_z and consider two gravel aquifers in Fig. 0 having
 387 arbitrary conductivities k_1 and k_2 . Here we assume that the interface between two gravel units of Fig. 0 is planar. This line is
 388 taken as the x -axis of a Cartesian coordinate system xBy (Fig. 6a).

389 There is a semi-circular lens of a radius R and conductivity k_3 placed as illustrated in Fig. 6a. Such lenses (a clayey one
 390 is shown in Fig. 0) are common sedimentary unconformities made of marl, mudrock, breccia or unconsolidated coarse
 391 sand.

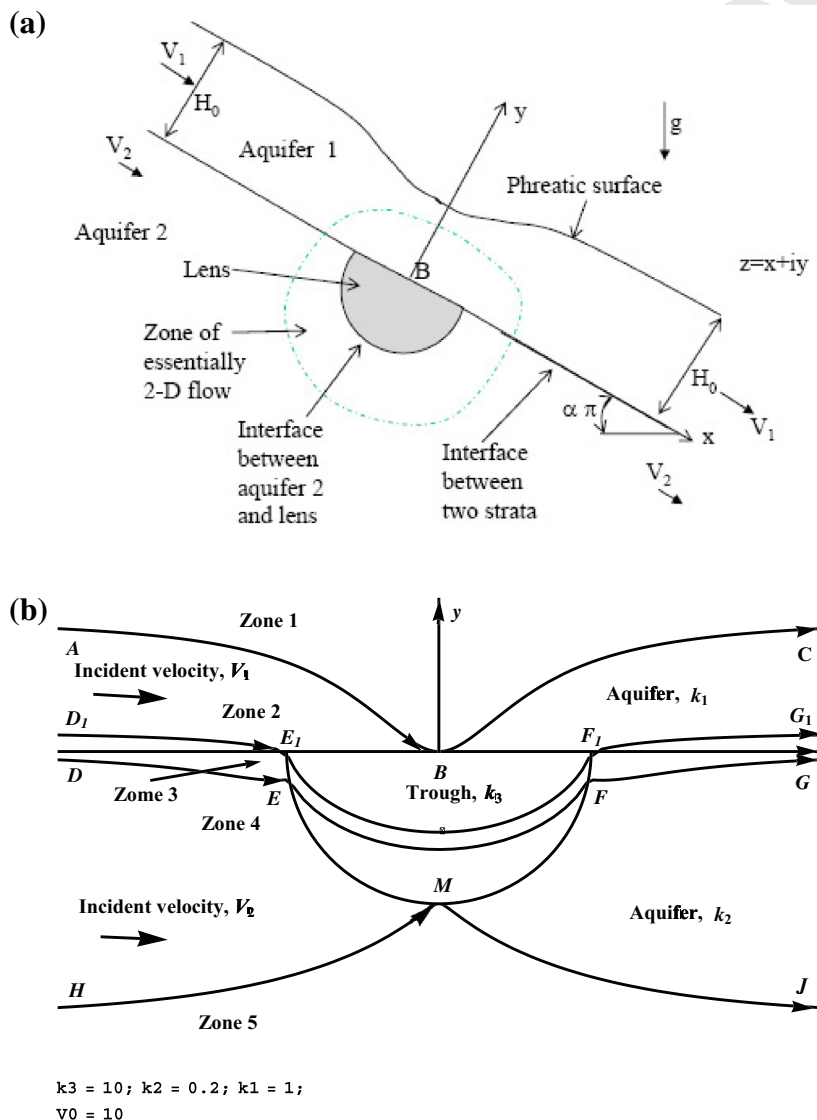


Fig. 6. Phreatic flow in a two-strata aquifer with a semi-circular lens (a); confined flow in a two-strata aquifer perturbed by a porous trough, $k_2/k_1 = 0.2$ and $k_3/k_1 = 10$ (b).

In a confined approximation to an unconfined flow of Fig. 6a we assume that both aquifers extend indefinitely in the y -direction (Fig. 6b), i.e. are bounded by bed-, cap-rock somewhere far from the x -axis. Solution to problem in Fig. 6b is close to one for Fig. 6a, provided α in Fig. 6a is sufficiently small.

Our main interest now is not the phreatic surface but flow across the interface and the role of the lens in the so-called “hydraulic commingling” for an arbitrary set k_1 , k_2 and k_3 . Without the lens in Fig. 6b the Darcian velocities in the two aquifers, \mathbf{v}_1 and \mathbf{v}_2 , are parallel to Bx and satisfy the condition

$$\frac{\mathbf{v}_1}{k_1} = \frac{\mathbf{v}_2}{k_2}, \tag{17}$$

i.e. seepage is piece-wise unidirectional and, consequently, the two strata are not commingled (no cross-flow through the abscissa axis). This 1-D, unidirectional flow we again call “normal”. The lens causes a nontrivial leakage from one stratum to another with refraction of the flow net on the interfaces between the three subdomains making the plane in Fig. 6b. Our aim is to examine the near-field (the lens vicinity) and to evaluate how much water circulates between aquifers 1 and 2.

The complexified Darcian velocities, $\mathbf{v}_1(z)$, $\mathbf{v}_2(z)$ and $\mathbf{v}_3(z)$ are antiholomorphic in the corresponding domains of Fig. 6b. As is well-known (PK62), the refraction conditions (continuity of the flux and pore pressure) consist of the proportionality of tangential and coincidence of normal components of $\mathbf{v}_j(z)$ at the corresponding parts of the interface:

$$\begin{aligned} k_2 \operatorname{Re} \mathbf{v}_1(x) &= k_1 \operatorname{Re} \mathbf{v}_2(x), & \operatorname{Im} \mathbf{v}_1(x) &= \operatorname{Im} \mathbf{v}_2(x), & |x| > R, \\ k_3 \operatorname{Re} \mathbf{v}_1(x) &= k_1 \operatorname{Re} \mathbf{v}_3(x), & \operatorname{Im} \mathbf{v}_1(x) &= \operatorname{Im} \mathbf{v}_3(x), & |x| < R; \\ k_3 \operatorname{Im}(\bar{t} \mathbf{v}_2(t)) &= k_2 \operatorname{Im}(\bar{t} \mathbf{v}_3(t)), & \operatorname{Re}(\bar{t} \mathbf{v}_2(t)) &= \operatorname{Re}(\bar{t} \mathbf{v}_3(t)), & |t| = R, \quad \operatorname{Im} t < 0. \end{aligned}$$

In terms of holomorphic functions $v_j(z) = \overline{\mathbf{v}_j(z)}$, $j = 1, 2, 3$, complex conjugated with the complexified velocities, the last conditions are equivalent to the following problem of \mathbb{R} -linear conjugation:

$$\begin{cases} v_1(x) = A_1 v_2(x) - B_1 \overline{v_2(x)}, & x \in (-\infty, -R) \cup (R, \infty), \\ v_2(x) = A_2 v_3(x) - B_2 \overline{v_3(x)}, & x \in (-R, R), \\ v_3(t) = A_3 v_2(t) + B_3 R^2 t^{-2} \overline{v_2(\bar{t})}, & |t| = R, \quad \operatorname{Im} t < 0, \end{cases} \tag{18}$$

where

$$A_j = \frac{k_1 + k_{j+1}}{2k_{j+1}}, \quad B_j = 1 - A_j, \quad j = 1, 2, \quad A_3 = \frac{k_3 + k_2}{2k_2}, \quad B_3 = 1 - A_3.$$

We fix the magnitude of $v_2(z)$ at infinity in the second aquifer by the condition $v_2(\infty) = V_0 > 0$. Then the velocity distribution in the three media is (see [27] for the details of derivations):

$$\begin{aligned} v_1(z) &= (e^{-i\pi\gamma} - \Delta_2 e^{i\pi\gamma}) V_1(z) + (e^{i\pi\gamma} - \Delta_2 e^{-i\pi\gamma}) V_2(z), \\ v_2(z) &= (1 + \Delta_1) [e^{i\pi(\lambda-\gamma)} V_1(z) + e^{-i\pi(\lambda-\gamma)} V_2(z)] + V_0 \Delta_1 \Delta_3 (1 - z^{-2}), \\ v_3(z) &= (1 + \Delta_2) [e^{-i\pi\gamma} V_1(z) + e^{i\pi\gamma} V_2(z)], \end{aligned} \tag{19}$$

where all parameters and functions $V_1(z)$, $V_2(z)$ are:

$$\Delta_1 = \frac{k_2 - k_1}{k_2 + k_1}, \quad \Delta_2 = \frac{k_3 - k_1}{k_3 + k_1}, \quad \Delta_3 = \frac{k_2 - k_3}{k_2 + k_3}, \tag{20}$$

$$e^{i\pi\gamma} = \frac{1}{2} \left(\sqrt{2 + \Delta_1 + \Delta_2} + \operatorname{isign} \Delta_3 \sqrt{2 - \Delta_1 - \Delta_2} \right), \tag{21}$$

$$e^{i\pi\lambda} = 1 - \Delta_3 \frac{\Delta_1 - \Delta_2}{2} + i|\Delta_3| \sqrt{1 - \left(\frac{\Delta_1 + \Delta_2}{2} \right)^2}, \tag{22}$$

$$\Lambda = \frac{V_0 \sin[\pi(\gamma - \lambda/2)]}{2(1 + \Delta_1) \cos(\pi\lambda/2) \sin(2\pi\gamma)}, \tag{23}$$

$$\begin{aligned} V_1(z) &= \Lambda \left\{ 1 - \frac{R^2}{z^2} + \left(\frac{R-z}{R+z} \right)^\lambda \left[1 + \frac{2\lambda R}{z} + \frac{R^2}{z^2} \right] \right\}, \\ V_2(z) &= \Lambda \left\{ 1 - \frac{R^2}{z^2} + \left(\frac{R+z}{R-z} \right)^\lambda \left[1 - \frac{2\lambda R}{z} + \frac{R^2}{z^2} \right] \right\}. \end{aligned} \tag{24}$$

Here the branch of the analytic function $[(R-z)/(R+z)]^\lambda$, equaled one at $z = 0$, is fixed in the z -plane with the branch cut along the half-circle $\{z : |z| = R, \operatorname{Im} z < 0\}$.

We introduce dimensionless quantities as $(x^*, y^*) = (x, y)/R$ and as usually drop (x, y) . We used the *Mathematica* routine **StreamPlot** and plotted the flow nets for $k_2/k_1 = 0.1$ and two trough conductivity ratios $k_3/k_1 = 0.5$ and $k_3/k_1 = 2.5$ (Fig. 7a and b, respectively, where arrowed curves are streamlines and dashed curves are equipotential lines).

Eight characteristic streamlines can be distinguished in Fig. 6b, plotted by *Mathematica* for $k_2/k_1 = 0.2$ and $k_3/k_1 = 10$. They demarcate (as separatrices) the capture zones induced by the lens. Flow is symmetric with respect to By and we will describe only its left half ($x < 0$). The curve AB in Fig. 6b separates the flow in aquifer 1 into a major part (Zone 1), which bypasses the lens, from the part, which enters the lens at $x < 0$ (and, of course, leaves it at positive x). Between AB and D_1E_1 (Zone 2) groundwater from aquifer 1 enters the lens but does not visit aquifer 2. Point E_1 is the triple point $x = -R, y = 0$ where all three interfaces (semicircle, its diameter and the ray) intersect. Between D_1E_1 and DE (Zone 3) aquifers 1 and 2 are commingled, i.e. groundwater from aquifer 1 crosses the ray $x < -R, y = 0$, visits aquifer 2 and then enters the lens. Asymptotically, DE approaches the x -axis at $x \rightarrow -\infty$. Zones 4 and 5 in the second stratum are similar to Zones 2 and 1, correspondingly. For the case of Fig. 7b we zoom out the zone where two strata commingle and portray the corresponding streamlines as Fig. 7c.

From (24) we get

$$\text{Im}v_1(x) = \begin{cases} \Lambda(\sin \pi(\gamma + \lambda) + \Delta_2 \sin \pi(\gamma - \lambda))(\rho_\lambda(x) - \rho_{-\lambda}(x)), & -\infty < x < -R, \\ \frac{V_0(1+\Delta_2) \sin \pi(\gamma-\lambda/2)}{4 \cos(\pi\lambda/2) \sin \pi\gamma} (\rho_\lambda(-x) - \rho_{-\lambda}(-x)), & -R < x < 0, \end{cases}$$

where

$$\rho_\lambda(x) = \left(\frac{x+R}{x-R}\right)^\lambda \left(1 - \frac{2R\lambda}{x} + \frac{R^2}{x^2}\right).$$

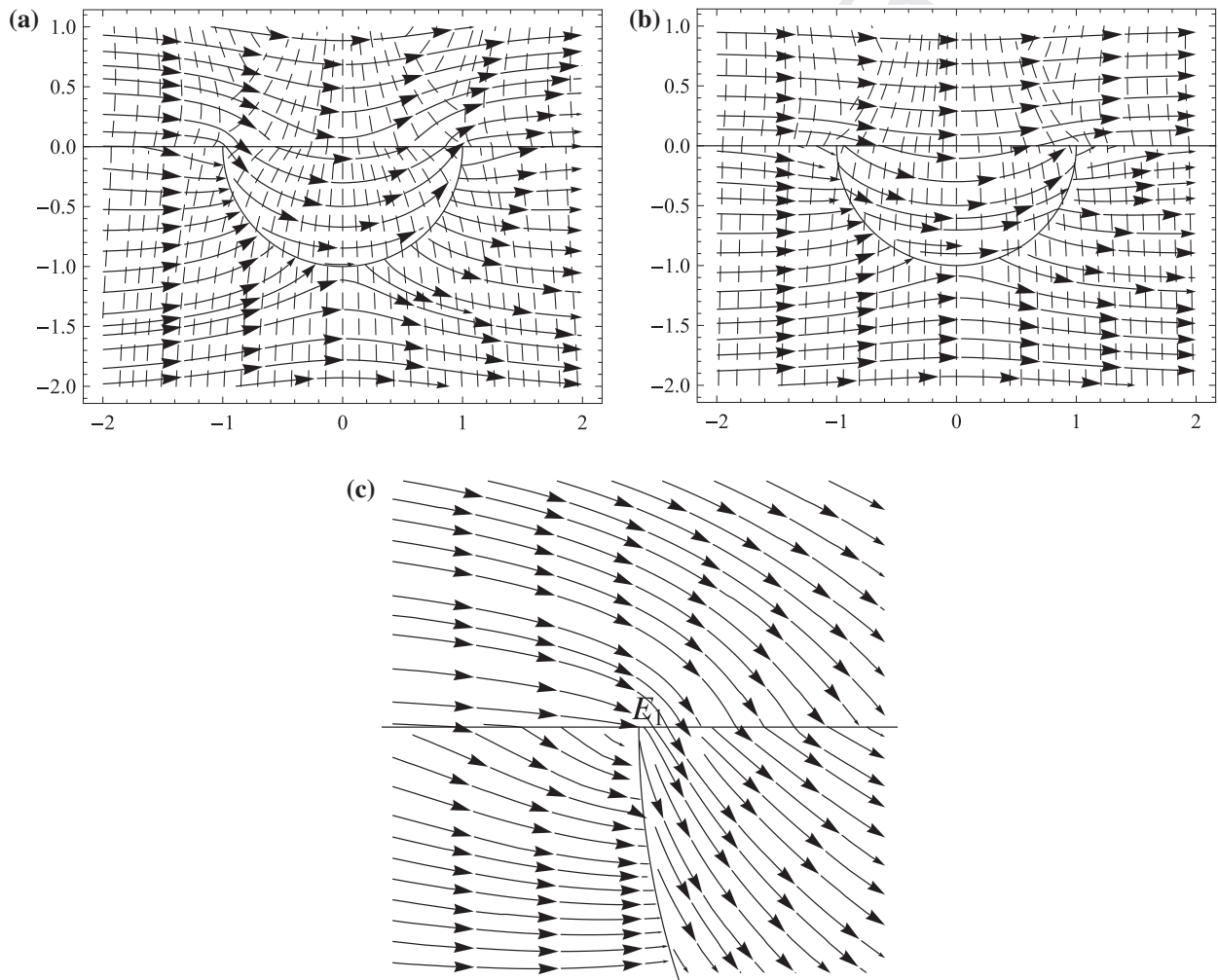


Fig. 7. Flow nets for $k_2/k_1 = 0.1$ and two trough conductivities $k_3/k_1 = 0.5$ (a) and $k_3/k_1 = 2.5$ (b); streamlines in a zoomed zone of commingling for $k_2/k_1 = 0.1$ and $k_3/k_1 = 2.5$ (c).

The representation for $\text{Im } v_1(x)$ at the interval $(-R, 0)$ was derived using the equality $\text{Im } v_1(x) = \text{Im } v_3(x)$.

The vertical component of v_1 along DE_1 and E_1B was used in the **NIntegrate** routine of *Mathematica* for evaluation of the flow rates through DE_1 and E_1B in Fig. 6b we introduce the corresponding dimensionless rates $Q_1 = Q_{DE_1}/(RV_0)$ and $Q_2 = Q_{E_1B}/(RV_0)$. In Fig. 8a we plot Q_1 as a function of k_3/k_1 for $k_2/k_1 = 0.01, 0.1, 0.9$ (curves 1–3). Fig. 8b shows $Q_2(k_3/k_1)$ for the same conductivity ratios. As the computations in Fig. 8a show, the commingling flow rate rapidly increases from zero at $k_3 = k_2$ to high values for lenses of relatively high permeability.

The intricate refraction of streamlines near point E_1 in Fig. 6b, 7c would be difficult to detect by standard MODFLOW-type tools. Similarly, the relatively small Q_1 and Q_2 are not easy to evaluate in mesh-based (FDM-FEM) codes. To a runner of a standard package, who deals with grid sizes in aquifer models (usually, on the catchment scale) much higher than the characteristic size R of a localized heterogeneity in Fig. 6a, attention to the vicinity of, say, point E in Fig. 6b, 7c may look like a supervacaneous niggling. In geotechnical and environmental engineering, however, the fine flow features near E and E_1 redound to the following:

- Suffosion and other types of micro-erosion of adjacent porous media is triggered by a non-trivial topology of streamlines and magnitudes of hydraulic gradients close to interfaces between media of contrasting conductivity–porosity (e.g., core-shoulder-base of a large earth-filled dam, see [43]). The above examined commingling makes possible exact evaluation of seepage forces (on the scale of REV involving such interfaces) and, consequently, a global analysis of stability of corresponding hydraulic structures.
- Well field downstream of the trough in Fig. 6a can tap groundwater from aquifer 1. Then commingling can seriously jeopardize the pumped water quality. Indeed, without the lens in Fig. 6a “a parallel -streamlines” regime and a “purely-aquifer-1” containment of groundwater take place. Topological divarications from “normality”, as illustrated in Figs. 7c and 8a and b, results in acquiring unwanted chemicals from the lens and aquifer 2, which is commonly of poorer quality from a hydrogeochemical viewpoint. Sometimes, even toxic substances from a clandestine buried waste repository can re-emerge by advection in aquifer 1. Vice versa, if a plume of contamination is rapidly propagating in a relatively highly-permeable aquifer 1, then one should be “hydraulically cautious” with remediation techniques. For example, in the upper aquifer of Wadi Suq (Batinah region of Northern Oman) there was an attempt to intercept a plume of DNAPL from a copper mining plant by constructing a backfield trench across the whole depth of aquifer 1 and partial embedding the trench into aquifer 2. The project failed because the plume, contained to aquifer 1 prior to installing the trench, “dived” into aquifer 2 when the trench started its operation. Groundwater motion (and therefore advective flushing) in aquifer 2 is slow and hence “pocketing” contaminants there, as Fig. 7c depicts, is detrimental. Our commingling model and flow nets in Fig. 7 qualitatively explain why the plume “dives”, even without any density effects.

To perpend the flow nets in Fig. 6a one really needs an arbitrarily-zoomable, absolutely exact velocity fields (19), from which hydrogeological, hydrological and environmental-engineering implications can be drawn.

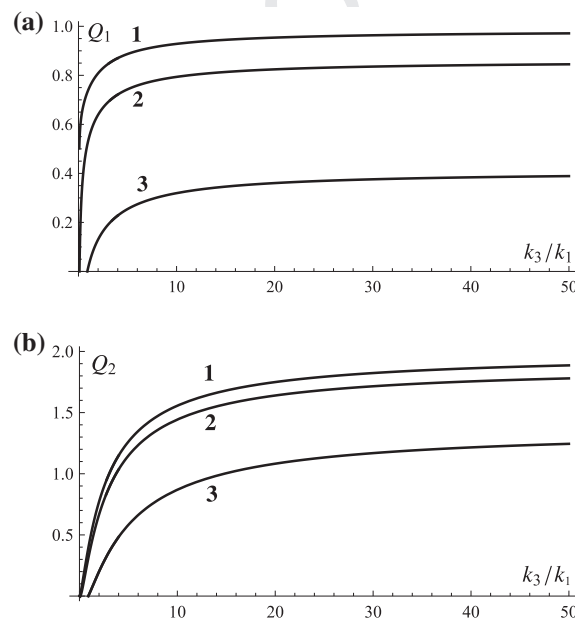


Fig. 8. Dimensionless flow rate $Q_1(k_3/k_1)$ through E_1E in Fig. 5b for $k_2/k_1 = 0.01, 0.1, 0.9$ (curves 1–3) (a); flow rate $Q_2(k_3/k_1)$ through EI in Fig. 5b for $k_2/k_1 = 0.01, 0.1, 0.9$ (curves 1–3) (b).

In this section the flow was generated by a dipole at infinity. Other types of driving point singularities (sinks, sources and multipoles) as well as elliptical, parabolic, hyperbolic and corner-shaped lenses, rather than the semi-circle of this section, have been recently investigated [44–47].

6. Conclusions

Aquifers/saturated soil layers in hillslope hydrology are often bounded from below by bedrock whose shape varies in space as in Fig. 0, reflecting the past geological events (e.g., tectonism). The hydraulic properties of the aquifer and bedrock also vary spatially, owing to geomorphological alterations, activity of plant roots, anthropogenic impacts, etc. In modeling of groundwater motion, however, simplifications related to the boundaries of flow domains and heterogeneity/anisotropy of porous media are needed to make the problem mathematically tractable. A standard assumption is that the bedrock is planar, its slope is constant and the hydrostratigraphic unit (a dipping stratum) is homogeneous with respect to hydraulic conductivity. In this paper we utilised the theory of holomorphic functions to obtain analytical solutions in terms of basic 2-D flow functions (the complex potential, Darcian velocity and Zhukovskii function) for an aquifer of an unconfined aquifer making a corner or curve. We also used a hydraulic model and compared the analytical solutions of the potential model with one obtained by numerical integration of a boundary value problem solved for a nonlinear ODE, which governs 1-D depth-averaged flow. We examined also a two-stratum aquifer with a trough whose hydraulic conductivity contrasts with those of the two layers between which the lens is sandwiched. We showed how the phreatic surface and separatrices, signifying the commingling effect of the trough, depend on the corner angles, shape of the aquifer, size of the trough and conductivity ratios.

In the potential model, by a conformal mapping of a circular triangle in the hodograph domain onto a complex potential strip or by the Cauchy-integral representations of solutions of inverse BVPs, a free (phreatic) boundary problem is explicitly and relatively easily solved. In fluid mechanics, purely analytical solutions to similar problems of open channel flows in terms of a full 2-D PT (ideal, irrotational flow of a heavy fluid with a specified non-planar channel bed) do not exist and simplifications (e.g. linearizations, ignoring gravity or assuming small disturbances to the “normal” free surface) or numerical (e.g. BEM) techniques are required to process integral equations. Analytically, only artificial solutions of Bervi and Zhukovskii [48,30] and Richardson are available in the full PT model (see, [38, pp. 460–468] for an overview). These antique “inverse” solutions are based on tinkering with mathematically fabricated “control” functions, which map the complex potential and hodograph plains onto an auxiliary domain with an exactly met nonlinear condition on the free surface and *a posteriori* obtained shapes of the channel bed. Groundwater flows are easier in this sense because along the phreatic surface (streamline) the velocity potential and vertical coordinate are linearly related (in open channel flows the squared velocity magnitude and vertical coordinate are linearly related). This allows tackling broad classes of bedrock geometries and using physically more meaningful “controls” (if the bedrock shape is “inversely” designed), albeit the Zhukovskii [36] idea has been also implemented by Gersevanov (PK62) in unconfined groundwater flows.

In phreatic flows, the bedrock “slope” is a controlling factor of the pore pressure and Darcian velocity fields, which are used in determining other fields (e.g., concentrations of advected chemicals, temperature, effective stresses, etc.) or kinematic characteristics (e.g., flow nets, isochrones, streaklines, etc.). Consequently, our solutions will be helpful in:

Catchment-scale assessment of runoff-baseflow, in particular, revealing the complex topology of subsurface storm-flow and dipping-reemerging pathlines in the mountain-region aquifers and vadose zone of Oman (applications to hydrology);

Seepage-induced liquefaction and slippage of saturated porous soil massifs over inclined impermeable or low-permeable strata (applications in geomorphology and geotechnical engineering);

Water uptake by the roots of phreatophytes growing on a relatively thin soil cover of a dipping impermeable rock with distinct ecotones controlled by the water table depth (application to hydroecology of mountain forests).

The illustrated excellent match between the 2-D analytical and 1-D numerical solution of Eq. (8) opens good perspectives for further juxtapositions of the two models. Indeed, integrating Eq. (8) for a geologically arbitrary non-planar bedrock geometry is relatively easy and many recently studied (see e.g., [49–51]) bedrock shapes underlying phreatic aquifers can be re-visited and re-examined.

Overall, modern methods and techniques for solving groundwater flow problems, as for example the boundary integral, finite difference and finite element methods can handle arbitrary boundary conditions (mixed, functionally dependent on x , t , etc.), whereas there are significant restrictions on most analytic techniques, especially the hodograph technique used above. The authors acknowledge the practical limitations of the used approaches but believe that there are also serious advantages: the insight of the intricate details of the flow topology, the ability to zoom out the flow net or phreatic surface shape to an arbitrary degree without refining the mesh (see e.g. [1] for details), avoidance of nuisance in satisfying the mass balance between cells of the mesh (typical in MODFLOW and other standard groundwater packages), as well as aesthetic and pedagogical value of elegant closed-form expressions. The analytical thinking, already pushed to catacombs of the modeling world, should not be completely eradicated by the juggernaut of purely numerical codes.

7. Main notations, abbreviations, nomenclature and synonyms. For potential referees only!

556 BVP – boundary value problem;
 558 DF – Dupuit–Forchheimer;
 559 DG – Dachler–Gersevanov;
 560 ODE – ordinary differential equation;
 561 PDE – partial differential equation;
 562 PK62 – [6];
 563 PT – potential theory;
 564 bedrock = aquifuge = impermeable bed;
 565 phreatic surface = water table = free surface;
 566 trough = lens = heterogeneity of a finite size;
 567 $f(x)$ = elevation of the phreatic surface over a curved bed in hydraulic model;
 568 F_1, F_2, F_3, F_4 = control functions of the aquifuge shape;
 569 g = gravity acceleration;
 570 G_z, G_w, G_v = physical, complex potential and hodograph domains (correspondingly);
 571 h = hydraulic head;
 572 H_0, H_1 = “normal” thicknesses of saturated zones;
 573 k, k_1, k_2, k_3 = hydraulic conductivities;
 574 $n = y - Y$ = new coordinate in the hydraulic model;
 575 p = pore pressure head;
 576 Q = flow rate;
 577 R = trough radius;
 578 \vec{V} = Darcian velocity vector;
 579 u, v = horizontal and vertical components of the Darcian velocity vector;
 580 U = depth-averaged velocity in the hydraulic model;
 581 $V = u + iv$ = complexified Darcian velocity vector;
 582 $w = \phi + i\psi$ = complex potential;
 583 x, y = cartesian physical coordinates;
 584 Y = elevation of the bedrock above $x = 0$ horizon;
 585 $z = x + iy$ = complex physical coordinate;
 586 $Zh = R_z + il_z$ – Zhukovskii function;
 587 $\alpha\pi, \beta\pi$ = angles of inclination of the aquifuge corner;
 588 ϕ = velocity potential;
 589 ψ = stream function;
 590 $\zeta = \xi + i\eta$ = auxiliary complex variable.

8. Uncited reference

593 ^{Q5} [52].

Acknowledgements

595 ^{Q6} This work was supported by the Grant SR/SCI/ETHS/11/01 “Estimating natural groundwater recharge and discharge in
 596 ^{Q7} North Oman”, His Majesty Research Trust Fund (Oman), and RFBR Grants No. 12-01-97015-r_povolgh’e_a, No. 13-01-
 597 00322 (Russia). Helpful comments by an anonymous referee are appreciated.

Appendix A. Derivation of governing equation in hydraulic model

598 In 2-D PT the horizontal, $u(x, y)$, and vertical, $v(x, y)$, velocity components are given by the Cauchy-Riemann relations:

$$600 \quad u = \frac{\partial \phi}{\partial x} = \frac{\partial \psi}{\partial y}, \quad v = \frac{\partial \phi}{\partial y} = -\frac{\partial \psi}{\partial x}. \quad (25)$$

603 Picard’s iteration technique provides successive approximations to u and v with the steps of an iterative cycle based on
 604 Eqs. (25), which are summarized for the “ i th-order” approximation for u as
 605

$$607 \quad u^{(i)} \rightarrow \psi^{(i)} = \int u^{(i)} dy \rightarrow v^{(i)} = -\frac{\partial \psi^{(i)}}{\partial x} \rightarrow \phi^{(i)} = \int v^{(i)} dy + F, \quad (26)$$

$$610 \quad u^{(i+1)} = \frac{\partial \phi^{(i)}}{\partial x} \rightarrow \psi^{(i+1)} = \int u^{(i+1)} dy \rightarrow Q = \psi^{(i+1)}(y = Y + f) \rightarrow F_x \rightarrow u^{(i+1)}.$$

It consist in successive partial integration and derivation with respect to the x - and y -coordinates, imposing in each cycle the boundary condition of the stream function at the free surface to determinate $F(x)$, where $F(x)$ is an integration function. The process is extensively described by Castro-Orgaz et al. [24]. Here we provide a detailed description for the first iteration $u^{(1)}$ and drop the superscript.

First, we introduce a new variable $n = y - Y(x)$ such that an arbitrary point P_i inside the flow domain in Fig. 1c has coordinates (x, n) for a given bedrock shape $Y(x)$. Next, we – as in the classical DF model – assume that the horizontal velocity u is constant in any vertical cross-section $y = const$. The depth-averaged velocity $U(x) = Q/f(x)$ where $f(x)$ is an unknown vertical elevation of the free surface above the bedrock.

Integration of the first of Eq. (25) in the vertical direction with x as constant gives:

$$\psi(x, y) = \int_{y_b}^y u(x, y) dy = \int_0^n u(x, n) dx = Un. \tag{27}$$

In this integration we took into account that $\psi = 0$ along the bedrock boundary $n = 0$.

We differentiate (27) with respect to x and get:

$$v = -\psi_x = -U_x n - Un_x. \tag{28}$$

Next, we integrate Eq. (25) with respect to x and insert (28) into the integrand:

$$\phi(x, y) = \int_{y_b}^y v(x, y) dy + F(x) = \int_0^n v(x, n) dn + F(x) = -U_x n^2/2 - Un_x n + F(x), \tag{29}$$

where $F(x)$ is a function to be found.

Now we differentiate (29) with respect to x

$$u = \phi_x = -U_{xx} n^2/2 - n(2U_x n_x + Un_{xx}) - Un_x^2 + F_x. \tag{30}$$

Now we integrate Eq. (25) with respect to y and insert (30) into the integrand:

$$\psi(x, y) = \int_{y_b}^y u(x, y) dy = \int_0^n u(x, n) dn = -U_{xx} n^3/6 - n^2/2(2U_x n_x + Un_{xx}) - Un_x^2 n + F_x n. \tag{31}$$

The unknown F_x is determined from the boundary condition of the stream function at the free surface:

$$\psi(x, n = f(x)) = Q. \tag{32}$$

Inserting Eq. (32) into Eq. (31) results in

$$F_x = U + U_{xx} n^2/6 + n/2(2U_x n_x + Un_{xx}) + Un_x^2. \tag{33}$$

Now we put F_x from Eq. (33) into Eq. (30) and eliminate the unknown function of integration:

$$u = U + U_{xx}(f^2/6 - n^2/2) + (2U_x n_x + Un_{xx})(f/2 - n). \tag{34}$$

Now we will follow the PK62 protocol and combine what Polubarinova-Kochina called the kinematic and isobaric boundary conditions on the phreatic surface. We recall that $\vec{V} = -k \text{ grad}h$ (Darcy's law) and $p = -\gamma - \phi/k$ (definition of the pressure head). From the last expression we get on the free surface

$$k(f + Y) = -\phi(x, f + Y) = U_x f^2 + Un_x f - F(x). \tag{35}$$

We combine (35) and (29) written on the phreatic surface and eliminate $F(x)$.

This transforms (29) into:

$$\phi = U_x(f^2 - n^2) + Un_x(f - n) - k(f + Y). \tag{36}$$

Eq. (36) is differentiated to obtain the horizontal velocity component u as

$$u = -k(f_x + Y_x) + U_{xx}/2(f^2 - n^2) + (Un_{xx} + U_x n_x)(f - n) + (f_x - n_x)Un_x + U_x(ff_x - nn_x). \tag{37}$$

Eq. (34) at the water table yields

$$u_s = U - (2U_x n_x + Un_{xx})f/2 - U_{xx} f^2/3, \tag{38}$$

whereas from Eq. (37) at the free surface, where $f = n$, we have

$$u_s = -k(f_x + Y_x) + (f_x - n_x)Un_x + U_x f(f_x - n_x). \tag{39}$$

Clearly, $U_x = -Qf_x/f^2$, $U_{xx} = -Qf_{xx}/f^2 + 2Qf_x^2/f^3$, $n_x = -Y_x$, $n_{xx} = -Y_{xx}$. We eliminate n and its derivatives from (38) and (39) and arrive at the final governing ODE (8) in the main body of the paper.

References

[1] O.D.L. Strack, Groundwater Mechanics, Prentice Hall, Englewood Cliffs, 1989.
 [2] X.S. Wang, S.P. Neuman, O.D.L. Strack, A. Verruijt, M. Jamali, B. Seymour, J. Bear, A.H.D. Cheng, C. Chen, X. Kuang, J.J. Jiao, Methods to derive the differential equation of the free surface boundary, Ground Water 49 (2011) 133–143, <http://dx.doi.org/10.1111/j.1745-6584.2010.00773.x>.

Please cite this article in press as: A. Kacimov et al., Groundwater flow in hillslopes: Analytical solutions by the theory of holomorphic functions and hydraulic theory, Appl. Math. Modell. (2014), <http://dx.doi.org/10.1016/j.apm.2014.11.016>

- [3] V.T. Chow, Open-Channel Hydraulics, McGraw-Hill, New York, 1959.
- [4] P. Forchheimer, *Hydraulik*, Teubner Verlags, Berlin, 1930.
- [5] G. Dagan, Second-order linearized theory of free-surface flow in porous media, *La Houille Blanche* 19 (8) (1964) 901–910.
- [6] P. Ya. Polubarinova-Kochina, Theory of Ground-water Movement, Princeton Univ Press, Princeton, 1962 (in Russian).
- [7] O. Castro-Organ, Steady free-surface flow in porous media: generalized Dupuit–Fawer equations, *J. Hydraul. Res.* 49 (1) (2011) 55–63.
- [8] O.A.E. Abdalla, M. Ali, K. Al-Higgi, H. Al-Zidi, I. El-Hussain, S. Al-Hinai, Rate of seawater intrusion estimated by geophysical methods in arid area of Al Khabourah, Oman, *Hydrogeol. J.* 18 (2010) 1437–1445, <http://dx.doi.org/10.1007/s10040-010-0606-0>.
- [9] P.G. Macumber, Lenses, plumes and wedges in the Sultanate of Oman: a challenge for groundwater management, *Dev. Water Sci.* 50 (2003) 349–370, [http://dx.doi.org/10.1016/S0167-5648\(03\)80031-X](http://dx.doi.org/10.1016/S0167-5648(03)80031-X).
- [10] A.R. Kacimov, Analytical solution and shape optimisation for groundwater flow through a leaky porous trough subjacent to an aquifer, *Proc. R. Soc. London A* 462 (2006) 1409–1423.
- [11] A.R. Kacimov, M.M. Sherif, J.S. Perret, A. Al-Mushikhi, Control of sea-water intrusion by salt-water pumping: coast of Oman, *Hydrogeol. J.* 17 (2009) 541–548, <http://dx.doi.org/10.1007/s10040-008-0425-8>.
- [12] P.G. Macumber, The cable tool program and groundwater flow in the Eastern Batinah alluvial aquifer, Sultanate of Oman, Report of the Ministry of Water Resources, 1998.
- [13] A.R. Kacimov, Analytical solution for a phreatic groundwater fall: the Riesenkampf and Numerov solutions revisited, *Hydrogeology J.* 20 (6) (2012) 1203–1209, <http://dx.doi.org/10.1007/s10040-012-0857-z>.
- [14] M.G. Anderson, T.P. Burt, Subsurface runoff, in: *Process Studies in Hillslope Hydrology*, Wiley, Chichester, 1990.
- [15] T.G. Chapman, R.F. Dressler, Unsteady shallow groundwater flow over a curved impermeable boundary, *Water Resour. Res.* 20 (10) (1984) 1427–1434.
- [16] I.F. Creed, G.Z. Sass, J.M. Buttle, J.A. Jones, Hydrological principles for sustainable management of forest ecosystems, *Hydrol. Processes* 25 (2011) 2152–2160, <http://dx.doi.org/10.1002/hyp.8056>.
- [17] M.E. Reid, R.M. Iverson, Gravity-driven groundwater flow and slope failure potential: 2. Effects of slope morphology, material properties, and hydraulic heterogeneity, *Water Resour. Res.* 28 (3) (1992) 939–950, <http://dx.doi.org/10.1029/91WR02695>.
- [18] E.M. Shaw, K.J. Beven, N.A. Chappell, R. Lamb, *Hydrology in Practice*, Spon Press, London, 2011.
- [19] P.A. Troch, C. Paniconi, E.E. van Loon, Hillslope-storage Boussinesq model for subsurface flow and variable source areas along complex hillslopes: 1. Formulation and characteristic response, *Water Resour. Res.* 39 (11) (2003) 1316, <http://dx.doi.org/10.1029/2002WR001728>.
- [20] R. Dächler, *Grundwasserströmung*, Springer, Wien, 1936.
- [21] N.M. Gersevanov, Application of functional analysis to solving problems of groundwater seepage, *Izv. AN SSSR OTN.* (7) (1943) 73–89 (in Russian).
- [22] A.R. Kacimov, Yu.V. Obnosov, Analytical solutions by the hodograph method to hydrodynamic problems for oil and gas traps, *J. Hydrol.* 254 (4) (2001) 33–46.
- [23] A.R. Kacimov, Yu.V. Obnosov, Accumulation of a light non-aqueous phase liquid on a flat barrier baffling a descending groundwater flow, *Proc. R. Soc. Lond. A* 468 (2012) 3667–3684, <http://dx.doi.org/10.1098/rspa.2012.0317>.
- [24] O. Castro-Organ, J.V. Giraldez, N. Robinson, Second order two-dimensional solution for the drainage of recharge based on Picards iteration technique: a generalized Dupuit–Forchheimer equation, *Water Resour. Res.* 48 (2012) W06516, <http://dx.doi.org/10.1029/2011WR011751>.
- [25] A.R. Kacimov, Yu.V. Obnosov, Analytical solution to 2D problem for an anticline-diverted brine flow with a floating hydrocarbon trap, *Transp. Porous Media.* 71 (1) (2008) 39–52, <http://dx.doi.org/10.1007/s11242-007-9110-y>.
- [26] A.R. Kacimov, H. Klammler, K. Hatfield, N.B. Ilyinsky, Constructural design of permeable reactive barriers: a groundwater hydraulics criterion, *J. Eng. Math.* 71 (4) (2011) 319–338, <http://dx.doi.org/10.1007/s10065-011-9457-5>.
- [27] Yu.V. Obnosov, Seepage refraction in a semicircular lens located at the boundary of two porous massifs, *J. Appl. Math. Mech.* 62 (5) (1998) 749–762, [http://dx.doi.org/10.1016/S0021-8928\(98\)00096-3](http://dx.doi.org/10.1016/S0021-8928(98)00096-3).
- [28] W. Li, Z. Liu, H. Guo, N. Li, W. Kang, Simulation of a groundwater fall caused by geological discontinuities, *Hydrogeol. J.* 19 (2011) 1121–1133, <http://dx.doi.org/10.1007/s10040-011-0747-9>.
- [29] S. Wolfram, *A System for Doing Mathematics by Computer*, Addison-Wesley, Redwood City, 1991.
- [30] B.J. Binder, F. Dias, J.-M. Van-Den-Broeck, Steady free-surface flow past an uneven channel bottom, *Theoret. Comput. Fluid Dyn.* 20 (3) (2006) 125–144, <http://dx.doi.org/10.1007/s00162-006-0017-y>.
- [31] J.S. Montes, Potential flow solution to 2D transition from mild to steep slope, *J. Hydraul. Eng.* 120 (50) (1994) 620–621, [http://dx.doi.org/10.1061/\(ASCE\)0733-9429\(1994\)120:5\(601\)](http://dx.doi.org/10.1061/(ASCE)0733-9429(1994)120:5(601)) (ASCE).
- [32] O. Castro-Organ, W.H. Hager, Critical flow: a historical perspective, *J. Hydraul. Eng.* 136 (3) (2010) 3–11, [http://dx.doi.org/10.1061/\(ASCE\)HY.1943-7900.0000158](http://dx.doi.org/10.1061/(ASCE)HY.1943-7900.0000158) (ASCE).
- [33] N.B. Ilyinsky, A.R. Kacimov, N.D. Yakimov, Analytical solutions of seepage theory problems. Inverse methods, variational theorems, optimization and estimates (a review), *Fluid Dyn.* 33 (2) (1998) 157–168.
- [34] A.R. Kacimov, Optimization and analysis of advective travel times beneath hydraulic structures, *J. Hydraul. Eng.* 134 (9) (2008) 1311–1317 (ASCE).
- [35] A. Verhoff, Generalized Poisson integral formula applied to potential flow solutions for free and confined jets with secondary flow, *Comput. Fluids* 54 (2012) 18–38.
- [36] N.E. Zhukovskii, Determination of fluid motion from a condition specified along a streamline, *J. Russ. Physico-Chem. Soc.* 12 (1891) 89 (in Russian).
- [37] D. Daboussy, F. Dias, J.M. Vanden-Broeck, Gravity flows with a free surface of finite extent, *Eur. J. Mech. B/Fluids* 17 (1998) 19–31.
- [38] M.I. Gurevich, Theory of Jets in Ideal Fluids, GIFML, Moscow, 1961 (Engl. transl.: 1965 Academic Press, New York).
- [39] A. Verhoff, Two-dimensional potential flow solutions with separation, *J. Fluid Mech.* 657 (2010) 238–264.
- [40] A.R. Kacimov, A.N. Nicolaev, Steady seepage near an impermeable obstacle, *J. Hydrol.* 138 (1992) 17–40.
- [41] A. Bejan, *Shape and Structure, From Engineering to Nature*, Cambridge University Press, Cambridge, 2000.
- [42] A.R. Kacimov, Yu.V. Obnosov, Analytical determination of seeping soil slopes of a constant exit gradient, *Zeitschrift für angewandte Mathematik und Mechanik* 82 (6) (2002) 363–376.
- [43] A.R. Kacimov, Yu.V. Obnosov, Analytical solutions for seepage near material boundaries in dam cores: the Davison–Kalinin problems revisited, *Appl. Math. Modell.* 36 (2012) 1286–1301, <http://dx.doi.org/10.1016/j.apm.2011.07.088>.
- [44] Yu.V. Obnosov, Solution of a R-linear conjugation problem on the case of hyperbolic interface, *Russ. Math.* (7) (2004) 53–62.
- [45] Yu.V. Obnosov, A generalized Milne–Thomson theorem, *Appl. Math. Lett.* 19 (2005) 581–586, <http://dx.doi.org/10.1016/j.aml.2005.08.006>.
- [46] Yu.V. Obnosov, A generalized Milne–Thomson theorem for the case of parabolic inclusion, *Appl. Math. Modell.* 33 (2009) 1970–1981, <http://dx.doi.org/10.1016/j.apm.2008.05.004>.
- [47] Yu.V. Obnosov, Three-phase eccentric annulus subjected to a potential field induced by arbitrary singularities, *Quart. Appl. Math.* 69 (2011) 771–786.
- [48] N. Bervi, On fluid motion with a free surface subject to gravity, *Proc. Division of Physical Sci., VI–VII, Imperial Soc. Natural Sci.*, 1894 (in Russian).
- [49] D.R. Steward, Groundwater response to changing water-use practices in sloping aquifers, *Water Resour. Res.* 43 (2007) W05408.
- [50] D.R. Steward, X. Yang, S. Chacon, Groundwater response to changing water use practices in sloping aquifers using convolution of transient response functions, *Water Resour. Res.* 45 (2009) W02412, <http://dx.doi.org/10.1029/2007WR006775>.
- [51] J. Zaidel, Discontinuous steady-state analytical solutions of the Boussinesq equation and their numerical representation by modflow, *Groundwater* (2013), <http://dx.doi.org/10.1111/gwat.12019>.
- [52] W.W. Read, Hillside seepage and the steady water table. I: theory, *Adv. Water Resour.* 19 (2) (1996) 63–73.